Cell Tissue Res (1998) 292:199–210

REGULAR ARTICLE

Andreas Bosio · Heinrich Büssow · Jutta Adam
Wilhelm Stoffel

Galactosphingolipids and axono-glial interaction in myelin of the central nervous system

Received: 25 September 1997 / Accepted: 7 November 1997

Abstract The myelin of central and peripheral nervous system of UDP-galactose-ceramide galactosyltransferase deficient mice (*cgt*$^{-/-}$) is completely depleted of its major lipid constituents, galactocerebrosides and sulfatides. The deficiency of these glycolipids affects the biophysical properties of the myelin sheath and causes the loss of the rapid saltatory conduction velocity of myelinated axons. With the onset of myelination, null mutant *cgt*$^{-/-}$ mice develop fatal neurological defects. CNS and PNS analysis of *cgt*$^{-/-}$ mice revealed (1) hypomyelination of axons of the spinal cord and optic nerves, but no apoptosis of oligodendrocytes, (2) redundant myelin in younger mice leading to vacuolated nerve fibers in *cgt*$^{-/-}$ mice, (3) the occurrence of multiple myelinated CNS axons, and (4) severely distorted lateral loops in CNS paranodes. The loss of saltatory conduction is not associated with a randomization of voltage-gated sodium channels in the axolemma of PNS fibers. We conclude that cerebrosides (GalC) and sulfatides (sGalC) play a major role in CNS axono-glial interaction. A close axono-glial contact is not a prerequisite for the spiraling and compaction process of myelin. Axonal sodium channels remain clustered at the nodes of Ranvier independent of the change in the physical properties of myelin membrane devoid of galactosphingolipids. Increased intracellular concentrations of free ceramides do not trigger apoptosis of oligodendrocytes.

This work was supported by the Deutsche Forschungsgemeinschaft, SFB 243 (Sto A4), the Fritz-Thyssen Foundation, the Stiftung Volkswagenwerk, and the Bundesministerium für Bildung, Wissenschaft, Forschung, und Technologie (BMBF) for the Center of Molecular Medicine Cologne (ZMMK, Förderkennzeichen 01 KS 9502).

A. Bosio · W. Stoffel (✉)
Molecular Neuroscience Laboratory, Institute of Biochemistry, Faculty of Medicine, University of Cologne,
Joseph-Stelzmann-Strasse 52, D-50931 Cologne, Germany
Tel.: +49–221–478–6881; Fax: +49–221–478–6882;
e-mail: Wilhelm.Stoffel@rs1.rrz.uni-koeln.de

H. Büssow · J. Adam
Anatomisches Institut, University of Bonn, Nussallee 10,
D-53115 Bonn, Germany

Key words Cerebrosides and sulfatides · Ceramide-galactosyl-transferase (CGT) · Ultrastucture of myelin · Sodium channel clustering · Dysmyelinosis · *Cgt*-knockout mouse

Introduction

Axons of the central (CNS) and peripheral nervous system (PNS) propagate excitation either by fast saltatory or slow continuous conduction. Saltatory conduction occurs in axons myelinated by oligodendrocytes in CNS and Schwann cells in PNS. Ion channels and ion pumps are concentrated in the axolemma at Ranvier's nodes. Myelin insulates axons by an increased capacitance and/or resistance of its lipid bilayer. The examination of naturally occurring mutants or artificially generated null-allelic mice have fostered our understanding of the function of the major myelin proteins (Boison and Stoffel 1994; Carenini et al. 1997; Giese et al. 1992; Klugmann et al. 1997; Li et al. 1994; Molineaux et al. 1986; Montag et al. 1994; Roach et al. 1985; Stoffel et al. 1997).

Approximately 70% of myelin dry weight consists of cholesterol and complex phospho- and glycolipids, among which the glycosphingolipids cerebrosides (galactosylceramide) and sulfatides (3-sulfo-cerebrosides) are oligodendrocyte and Schwann-cell specific. The isolation and characterization of rat UDP-galactose-ceramide galactosyltransferase (CGT) protein and its cDNA (Schulte and Stoffel 1993, 1995) and the murine and human CGT genes (Bosio et al. 1996a,b; Coetzee et al. 1996b) led to the generation of a CGT-null mutant mice (*cgt*$^{-/-}$) (Bosio et al. 1996c; Coetzee et al. 1996a). The deficiency of the myelin sheath of GalC and sGalC severely affects the biophysical properties of the lipid bilayer (Bosio et al. 1998). Consequently, the conduction velocity of PNS fibers in *cgt*$^{-/-}$ mice is reduced to that of unmyelinated axons. Neither the extent nor the compaction and periodicity of PNS myelin of *cgt*$^{-/-}$ mice was different from the wild type. The normal morphology of myelin of peripheral nerves suggested that the reduced conduction velocity is

mainly due to altered biophysical properties of the myelin sheath, which cause changes in the permeability of the bilayer. The *cgt*$^{-/-}$ mouse resembles a new model of severe dysmyelinosis. A regional hypomyelination in dorsal and ventral white matter of the spinal cord and a regional instability and vacuolation in the ventral columns of spinal white matter has been reported (Coetzee et al. 1996a).

We investigated the impact of the GalC/sGalC deficiency on the myelin structure of CNS and PNS axons at the ultrastructural level. A prominent symptom of dysmyelinosis is the loss of saltatory conductance of PNS axons. The reduced conduction velocity of *cgt*$^{-/-}$ PNS axons, which approaches that of unmyelinated axons, suggested a diffusion of sodium channels along the axons, which might be accompanied by a redistribution of sodium channels along the axon. These channels are normally clustered in the nodes of Ranvier. Structural changes of the nodes of Ranvier of peripheral axons were analyzed by electron microscopy and complemented by immunocytochemical analyses using sodium-channel-specific monoclonal antibodies. Sodium channels remained clustered in the nodal area. Therefore, glycosphingolipids are not responsible for the clustering of sodium channels in myelinated PNS axons.

Materials and methods

Animals

The generation of the *cgt*$^{-/-}$ mouse line has been described before (Bosio et al. 1996c). *cgt*$^{-/-}$ mice were killed between p14 and p70 for electron microscopy and immunocytochemistry.

Apoptosis test

p14 and p19 wild type, hetero-, and homozygous littermates of CGT-deficient mice were sufficated in a CO_2 atmosphere and then perfused with 20–40 ml of 4% paraformaldehyde in PBS through the left cardiac ventricle. Brains were excised and postfixed for 4 h in the same fixative and then incubated in 0.5 M sucrose overnight. Brains were frozen and embedded in Tissue-Tek O.C.T. Compound (Miles, Elkart, USA). Thin sections were analyzed for apoptotic cells using the ApopTag in situ apoptosis-detection kit (Oncor, Gaitherburg, USA) following the modified descriptions of the manufacturer: sections were permeabilized in a 0.1% Triton/0.1% sodium-citrate solution on ice for 2 min in a Coplin jar and subsequently rinsed twice with PBS for 5 min each before quenching of endogenous peroxidase with 1% hydrogen peroxide for 10 min. Color development was performed by staining with diaminobenzidine (DAB) as a substrate (Boehringer Mannheim) for 5–15 min. Specimens were mounted on gelatine-coated coverslips.

Light and electron microscopy

Mice were anaesthesized with Nembutal and perfused with 6% glutaraldehyde via the left cardiac ventricle. Segments of the spinal cord, optic, and sciatic nerve were obtained, postfixed in 1% phosphate-buffered OsO_4 in 0.1 M sucrose, and embedded in Epon 812. Semithin sections were stained with toluidine/pyronin as described before (Büssow 1978). Ultrathin cross sections of the spinal cord, optic, and sciatic nerve were contrasted with uranylacetate and lead citrate and examined as described before (Büssow 1978).

Immunolabeling of sodium channels

Immunolabeling was carried out as described before (Dugandzija-Novakovic et al. 1995). Mouse sciatic nerve was incubated in collagenase/dispase (Sigma, Deisenhofen, Germany, 3.5 mg/ml) for 60 min at 37°C. Nerves were placed on coverslips which had been coated with three parallel stripes of Cell-Tak (Collaborative Biomedical Products, Becton Dickinson, Bedford, USA). Nerve fibers were gently separated with fine needles from each other. After fixing in 4% paraformaldehyde, the samples were rinsed in 0.05 M phosphate buffer (PB), pH 7.4, and dried 5 min at 37°C. Axons were preincubated in 0.1 M PB, pH 7.4, containing 0.3% Triton X-100 and 10% bovine serum albumin (BSA, Sigma) (PBTB) for 1.5 h at room temperature (RT). The primary anti-Na^+ channel (III-IV linker region, rabbit affinity purified IgG, Upstate Biotechnology, Lake Placid, USA) antibodies were added in a 1:50 dilution and incubated for 15 h at RT. Then second antibody (biotinylated goat anti-rabbit IgG, Sigma, 1:200, 1 h, RT) followed by streptavidin-Cy3 conjugate (Sigma S6402, 1:400, 1 h, RT) were added. Samples were rinsed with PBTB 3 times for 15 min each. Finally, axons were rinsed with 0.05 M PB, dried, and mounted with gelatine on coverslips.

Results

Hypomyelination in CNS of CGT-deficient mice

Light microscopy of semithin cross sections through the ventral funiculi of cervical spinal cord of *cgt*$^{-/-}$ mice revealed hypomyelination of the CNS (Fig. 1a–d). A reduced number of ensheathed axons as well as an overall reduced thickness of individual myelin sheaths wrapping axons of a given size contributed to the hypomyelination in the CNS of *cgt*$^{-/-}$ mice. This observation is in agreement with a previous report (Coetzee et al. 1996a). However, hypomyelination is not confined to the spinal cord of *cgt*$^{-/-}$ mice. Figures 1e,f and 2a–c revealed a similar morphology in cross sections of the intraorbital portion of the optic nerves of p34 *cgt*$^{-/-}$ mice. The number of myelinated axons was smaller. No discrepancy between axon diameter and myelin thickness was observed as reported for myelin of spinal cord axons of *cgt*$^{-/-}$ mice.

Redundant myelin forms vacuolated fibers in the CNS myelin of *cgt*$^{-/-}$ mice

A striking abnormality of myelin of central nervous system of *cgt*$^{-/-}$ mice was a distorted axon-to-fiber diameter. The myelin sheath did not tightly wrap around the axon,

Fig. 1 Semithin cross sections through the ventral funiculi of cervical spinal cords of littermates (p34) show the hypomyelination of the *cgt*$^{-/-}$ mutant (**b**) in comparison with the wild type (**a**). High-power light microscopy of corresponding fiber tracts bordering the anterior median fissure (*arrowhead*) shows that the CNS axons of the mutant (**d**) have a marked reduction of their myelin sheath as compared to the wild-type fibers (**c**). Cross sections through the intraorbital portion of the optic nerves of age-matched control mice (p34, **e**). Nearly all axons are ensheathed with myelin, whereas in the optic nerve of the *cgt*$^{-/-}$ mouse (p34, **f**), the myelinated fibers are reduced in number. *Scale bars* **a, b** 100 μm, **c–f** 16 μm

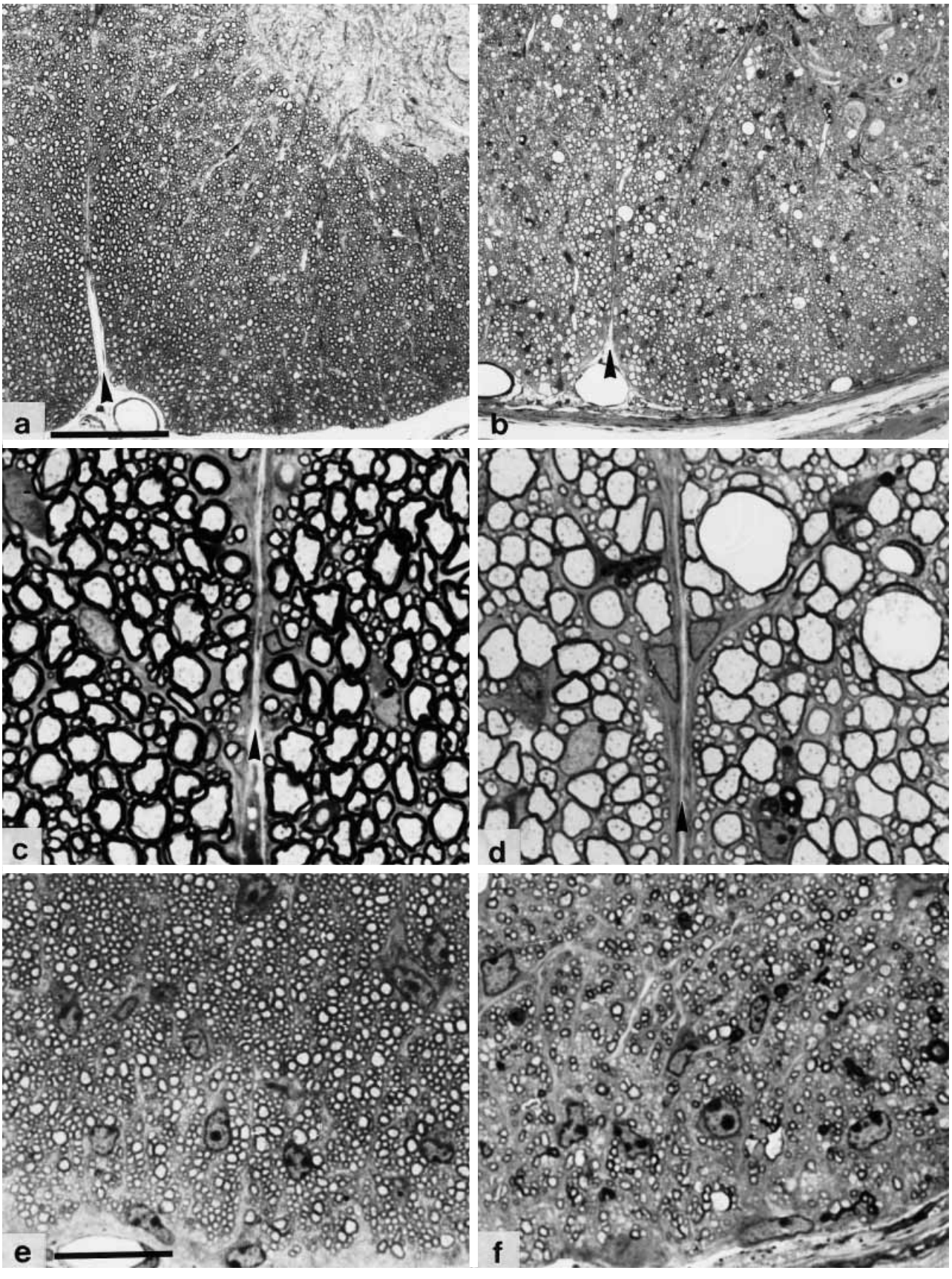

Fig. 1a–f

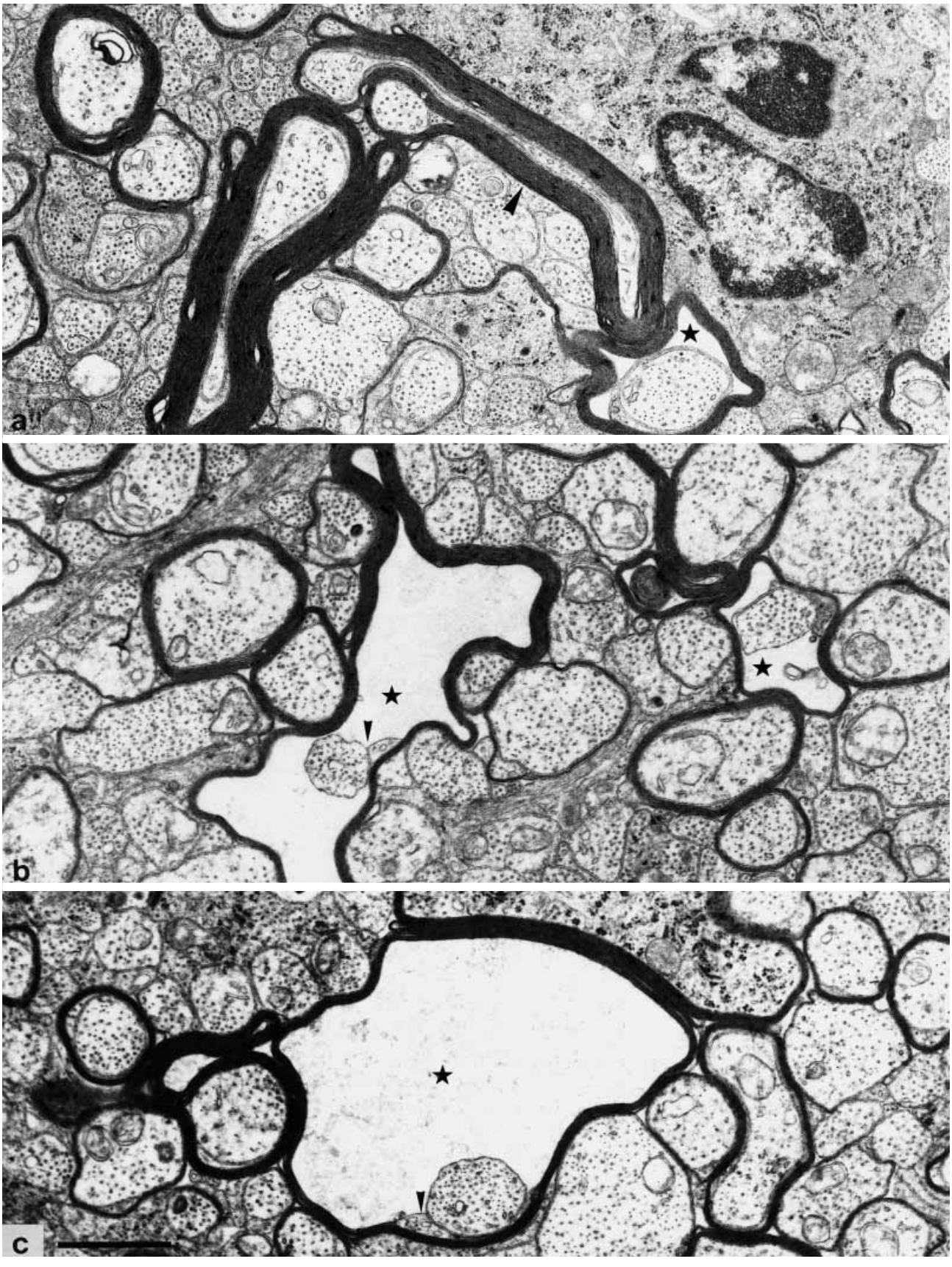

Fig. 2a–c

but was separated from the axolemma by a wide space. Redundant myelin formed highly disordered myelin loops in developing mice. In young mice, the abundant myelin was tightly folded as shown in cross sections of *cgt*$^{-/-}$ p23 optic nerves (Fig. 2a). Moreover, outer sheaths of the myelin bilayer of two different oligodendrocytes or two different processes of the same oligodendrocyte formed a interperiod dense line. Occasionally, the redundant myelin enclosed a second myelinated axon or glial cell body. Redundant myelin was only rarely observed in normal CNS. As some *cgt*$^{-/-}$ mice reached an age of 30–40 days, the redundant myelin might form so-called "split myelin sheaths", dissociated from the targeted axon and inflated by extracellular fluid, which expands the myelin sheath to vacuolated fibers (Fig. 2b,c). The axon-oligodendrocyte contact was restricted to the inner loops. Several intermediate stages between redundant myelin and vacuolated fibers could be observed. The compaction of the myelin sheaths was not affected.

Multiple myelinated axons in the CNS of *cgt*$^{-/-}$ mice

Besides redundant myelin and vacuolated fibers, another pathological structure in CNS myelin of *cgt*$^{-/-}$ mice were atypical structures in oligodendrocytic cytoplasm (Fig. 3). In some cases, these myelin loops were oriented in the same direction (Fig. 3b). They represented the inner and outer loop of two concentric myelin sheaths spiraling around one single axon in opposite directions. In other cases, they oppose each other (Fig. 3c). This morphology may result from two different myelin sheaths having wrapped around one axon in the same direction, which brought an inner and an outer loop in opposite positions, or it may haven arisen from the same sheath carrying an incisure parallel to the inner and outer loop of the sheath (Hirano and Dembitzer 1967). Both myelin sheaths built a normal interperiod dense line at their contact surface.

CNS of *cgt*$^{-/-}$ mice exhibit abnormal structure of paranodal loops

Cross sections of the paranodal region of the multiply myelinated axons of *cgt*$^{-/-}$ mice showed structures resembling Lanterman incisures (Fig. 4a). However, longitudinal sections unambiguously revealed three unusual morphological features: (1) paranodal loops not contacting the axolemma, but terminating on an underlying myelin sheath of a different paranode (Fig. 4b), (2) loops pointing in opposite directions, which prohibits their adherance to the axolemma (Fig. 4b), and (3) one of the innermost lateral loops being elongated (Fig. 5a,b). Thus, they extended along the axolemma in the periaxonal space and prohibited a direct axo-glial contact of the outer lateral loops, which was not observed in wild type (Fig. 5c).

Fig. 2 Electron micrographs of cross sections through the optic nerves of *cgt*$^{-/-}$ mutant mice (**a** p23, **b, c** p34). Axons are often devoid of their myelin sheath. The diameter of the myelin sheaths greatly exceeds the diameter of axons. "Redundant" myelin (*arrowhead*) can be observed in younger mutant mice (**a**). The CNS nerve fibers of older animals (**b, c**) often show vacuolated fibers (*asterisk*). Here the axon-oligodendrocyte contact is restricted to the inner loops of the internode (*arrowhead*). There are numerous morphological intermediates between redundant myelin and vacuolated fibers (*asterisk*) ■. *Scale bar* 1.2 μm

Normal ultrastructure of the PNS

In contrast to myelinated nerve fibers of the CNS, the morphology of PNS myelin appeared completely unaffected as far as its structure and organization was concerned (Fig. 6).

The distribution of sodium channels in the axolemma of myelinated fibers of the PNS of *cgt*$^{-/-}$ and wt mice is unaltered.

Sciatic nerves of p20, p56, and p70 wild type and *cgt*$^{-/-}$-mice were dissected and fixed on coverslides for immunocytochemistry of sodium channels. They were permeabilized and labeled with an anti-Na^+-channel antibody followed by second antibody and streptavidin-Cy3 conjugate. This antibody binds specifically to sodium channels of myelinated PNS axons (Dugandzija-Novakovic et al. 1995; Novakovic et al. 1996; Vabnick et al. 1996).

Figure 7 illustrates the sharp and distinct immunolabelling of sodium channels of wt and *cgt*$^{-/-}$ sciatic nerve fibers which was restricted to the nodal region of myelinated axons. The internodal regions of axons of wild type or *cgt*$^{-/-}$ mice remain unlabeled. Unmyelinated axons showed a continuous labeling of the axolemma (not shown).

Apoptosis is not observed in hypomyelinated CNS of *cgt*$^{-/-}$-deficient mice

The observed hypomyelination in the CNS of *cgt*$^{-/-}$ mice as well as previously reported elevated amounts of ceramide suggested the possibility of apoptosis of oligodendrocytes of *cgt*$^{-/-}$ mice (Bosio et al. 1998). We analyzed cryosections of brains of p14 and p19 wild-type hetero- and homozygous *cgt*$^{-/-}$ littermates with the ApopTag in situ apoptosis-detection kit (Oncor). Apoptotic cells were neither observed in wild type nor in heterozygous or homozygous *cgt*$^{-/-}$ mice sections (not shown).

Fig. 3a–c Cross sections through white matter of the spinal cord of *cgt*$^{-/-}$ mice (p34). Internodes show inclusions of the oligodendrocytic cytoplasm in the compacted myelin sheaths (*arrowhead*). Two distinct myelin sheaths wrap the axon either in opposite (**b**) or in the same direction (**c**). *Scale bars* **a** 1.2 μm, **b, c** 0.36 μm ▶

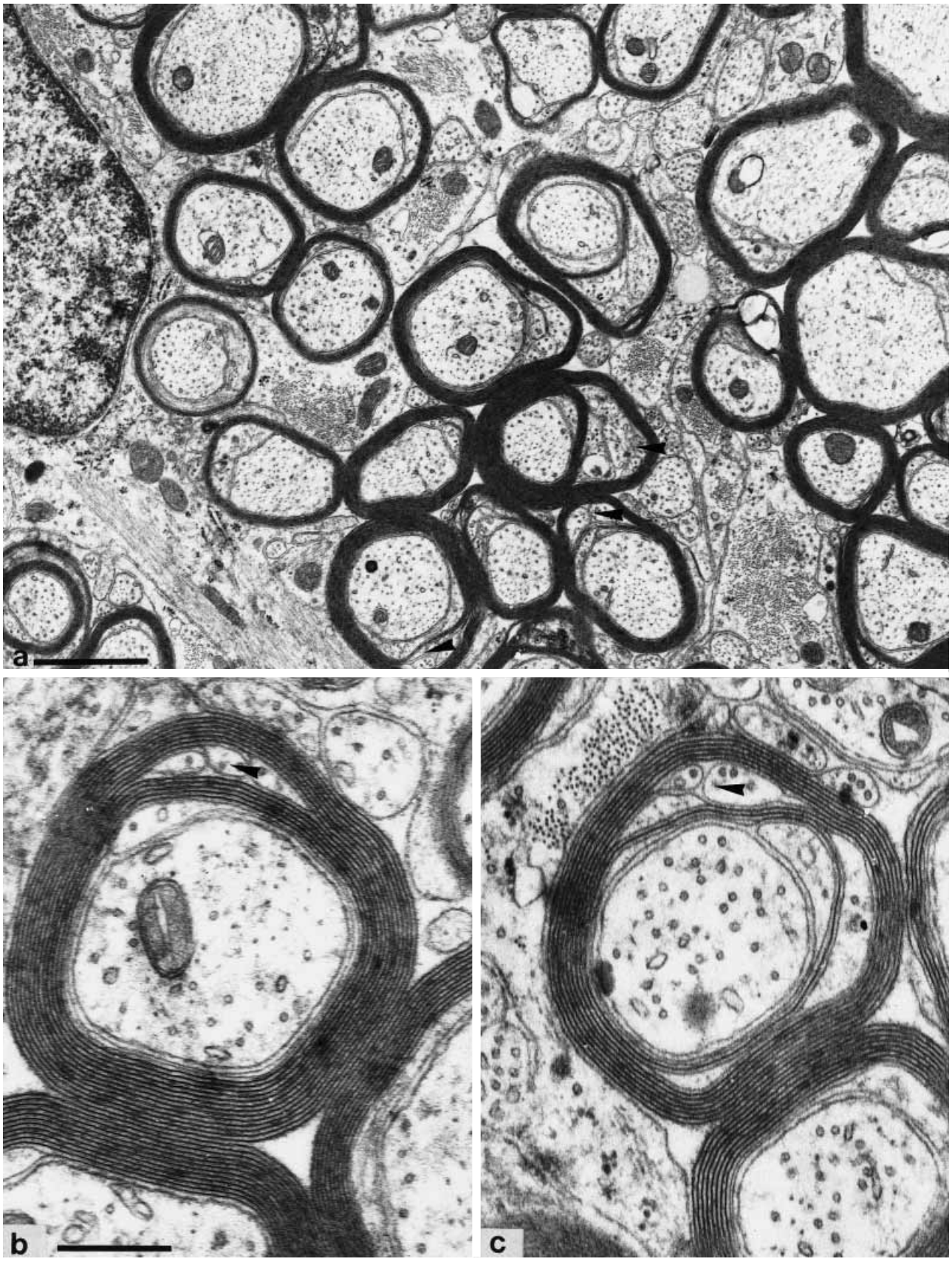

Fig. 3a–c

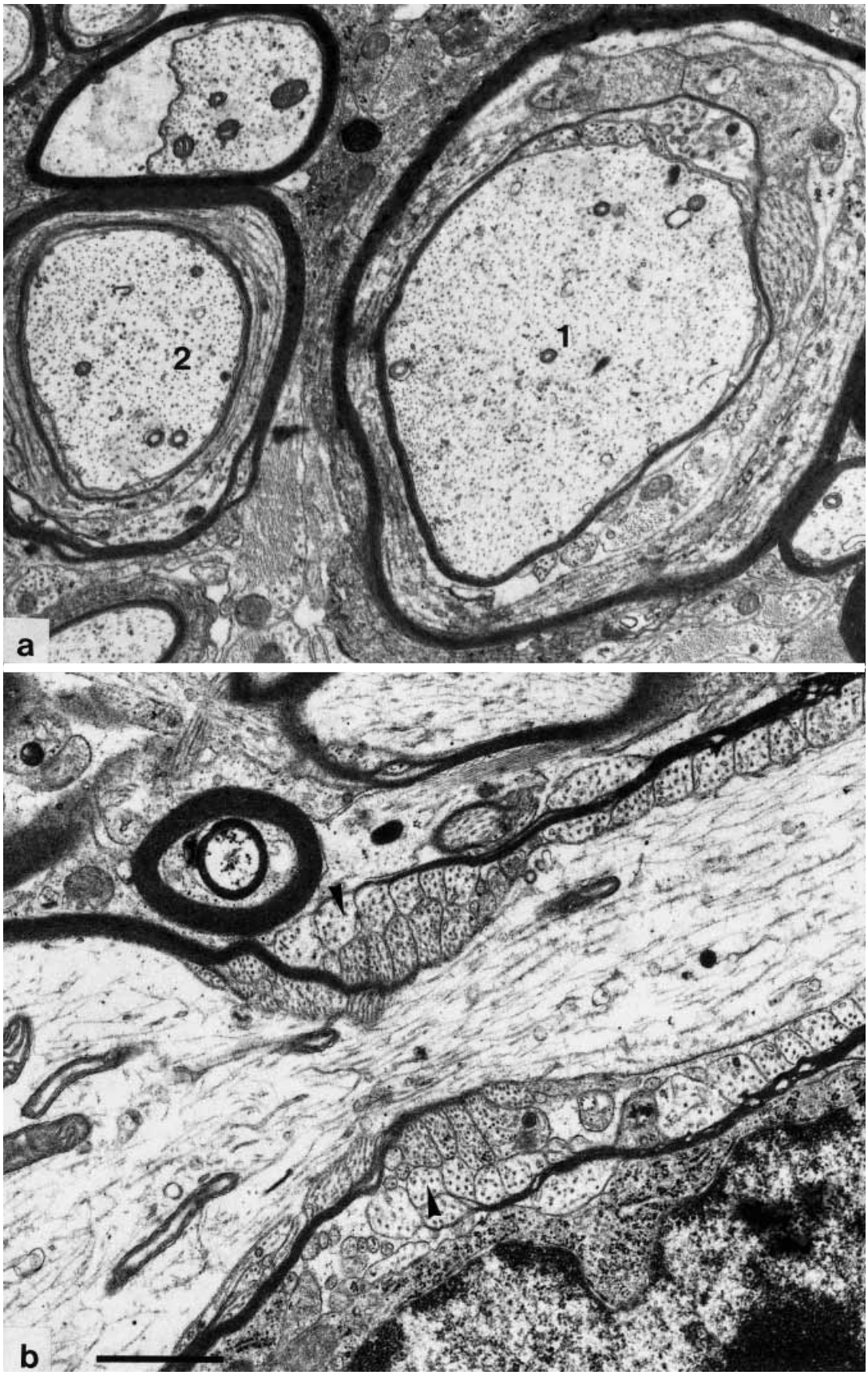

Fig. 4a–b

Discussion

Galactocerebrosides (GalC) and sulfatides (sGalC) are abundant in the myelin sheath and have unique structures and properties. The pivotal step in the biosynthesis of the galactocerebrosides has been unraveled by purification of the UDP-galactose ceramide galactosyltransferase (CGT) and cloning of its cDNA (Schulte and Stoffel 1993). The subsequent generation and analyses of CGT-deficient mice ($cgt^{-/-}$) allowed the first in vivo study of the function of GalC and sGalC. The phenotype of $cgt^{-/-}$ mice which develops during the myelination period, with its neurological symptoms and the electrophysiological findings resemble those of a new form of dysmyelinosis. The myelin sheath of PNS axons is structurally normal but functionally defective. Therefore, the impact of GalC/sGalC deficiency on the function of the myelin suggests the following molecular interpretation of the major intrinsic properties of GalC/sGalC in the myelin lipid bilayer: (1) amide-bonds, carboxy-, and hydroxyl-groups in the interface of the hydrophobic core and the polar head group form an extensive net of hydrogen bonds. (2) The very long and mostly saturated fatty acids contribute to the stable, compacted hydrophobic core. (3) The polar head groups of GalC and sGalC contribute to a highly polar and negatively charged surface (O'Brien and Rouser 1964; Curatolo 1987; Pascher et al. 1992). It is obvious that the loss of these oligodendrocyte- and Schwann-cell-specific galactosphingolipids renders the myelin membrane less condensed leading to a high conductivity and/or small capacity of the multilayered myelin sheath (Bosio et al. 1998).

Ultrastructurally, we found three aberrant structures of CNS myelin: (1) "redundant" myelin, (2) a random targeting of existing myelin sheaths by other oligodendrocyte plasma membrane processes, and (3) interdigitation of paranodal loops of adjacent internodes, which reduce nodal regions to so-called pseudo-nodes. The structure and function of GalC/sGalC in CNS myelin may be regarded as the underlying principle of these three morphological features. GalC/sGalC in the outer surface of the plasma membrane might interact with complementary structures on the axolemma and directly or cooperatively recognize axolemma surfaces. The altered architecture of paranodes could result from a deficiency in the surface of oligodendrocytes of molecules required for the interaction with counterparts in the axolemma. GalC/sGalC could act as an adhesion/receptor molecule coupled to a secondary signal system. Several previous observations support this molecular interpretation (Bansal and Pfeiffer 1989; Bansal et al. 1988; Diaz et al. 1978; Dorfman et al. 1979; Owens and Bunge 1990; Raine et al. 1978; Ranscht et al. 1982, 1987; Roberts 1986).

The GalC/sGalC are accumulated in the outer leaflet of the myelin bilayer and could contribute to the lateral surface pressure of the myelin membrane. Their special physical properties could lead to the cluster formation with cholesterol within the membrane with or without the association of integral or peripheral membrane proteins. These rafts could interact with complementary structures of an apposing membrane (Simons and Ikonen 1997).

Oligodendrocytes and Schwann cells of $cgt^{-/-}$ mice produce abundant amounts of glucocerebrosides, which insufficiently compensate for the loss of galactocerebrosides. Glucosyl-transferase uses ceramides with hydroxy-fatty acyl residues, which are normally only found in GalC and sGalC as acceptor substrates, but are abundant in the $cgt^{-/-}$ mouse. Interestingly, only Schwann cells but not oligodendrocytes transfer a sulfate group to the newly formed glucocerebrosides. Sulfated glucocerebrosides are normally absent in PNS myelin, but in the $cgt^{-/-}$ mouse, it amounts to approximatly 40% of the total sGalC present in wild type mice (Bosio et al. 1996c, 1998). Some of the abnormal myelin structures reported here have also been observed in myelin-associated glycoprotein (MAG)-deficient mice: redundant myelin, multiple myelinated axons, as well as disorientated paranodal loops (Li et al. 1994; Montag et al. 1994). MAG-deficient mice, however, have a normal conduction velocity. Whether sulfatides and the carbohydrate epitope L2/HNK-1 of MAG exert comparable and redundant functions remains to be elucidated.

Sodium channels are clustered in Ranvier's nodes of myelinated axons. Here they are present in a 25× higher concentration than in the internodal region (Waxman and Ritchie 1993; Black et al. 1990). We studied the localization of these channels in $cgt^{-/-}$ peripheral axons by immunostaining. It has been shown in vivo and in vitro that Schwann cells induce the clustering of sodium channels along the axolemma (Dugandzija-Novakovic et al. 1995; Joe and Angelides 1992; Vabnick et al. 1996). In CNS axolemma, this channel clustering depends on a protein secreted by oligodendrocytes (Kaplan et al. 1997). The clustering process thus far is not understood in molecular terms (for a review, see Salzer 1997).

Our results clearly show that no gross redistribution of sodium channels in axolemmate ensheathed with a structurally apparently unaffected, but dysfunctioning myelin membrane occurs in the CGT deficient mouse, nor are cerebrosides and sulfatides required for the aggregation of sodium channels in the nodes of peripheral nerves. The

◀ **Fig. 4** Electron micrographs of a cross section (**a**) and a longitudinal section (**b**) through paranodal regions of CNS nerve fibers in the spinal cord of $cgt^{-/-}$ mice (**a** p34, **b** p23). Cross sections of multiple myelinated axons (*1*) differ from that of nerve fibers sectioned in the region of a Schmitt-Lanterman incisure (*2*). Only the longitudinal section (**b**) unequivocally shows two oligodendrocytic myelin sheaths layered on top of each other. They envelop one axon and terminate in lateral loop-like structures (*arrowhead*). *Scale bars* 1.2 μm

Fig. 5 Longitudinal sections through nodal and paranodal regions of CNS fibers in the spinal cord of p23 (**a**) and p34 (**b**) $cgt^{-/-}$ mice. The lateral loops of the oligodendrocyte do not contact the axolemma. They terminate on the innermost axonal cytoplasmic collar of the oligodendrocyte (*arrowhead*). **c** Node and paranode of myelin of optic nerve of p34 wild type CNS. The axoglial junctions between the lateral loops of the oligodendrocyte and the axolemma are indicated by an *arrowhead*. *Scale bars* **a** 1.2 μm, **b, c** 0.36 μm

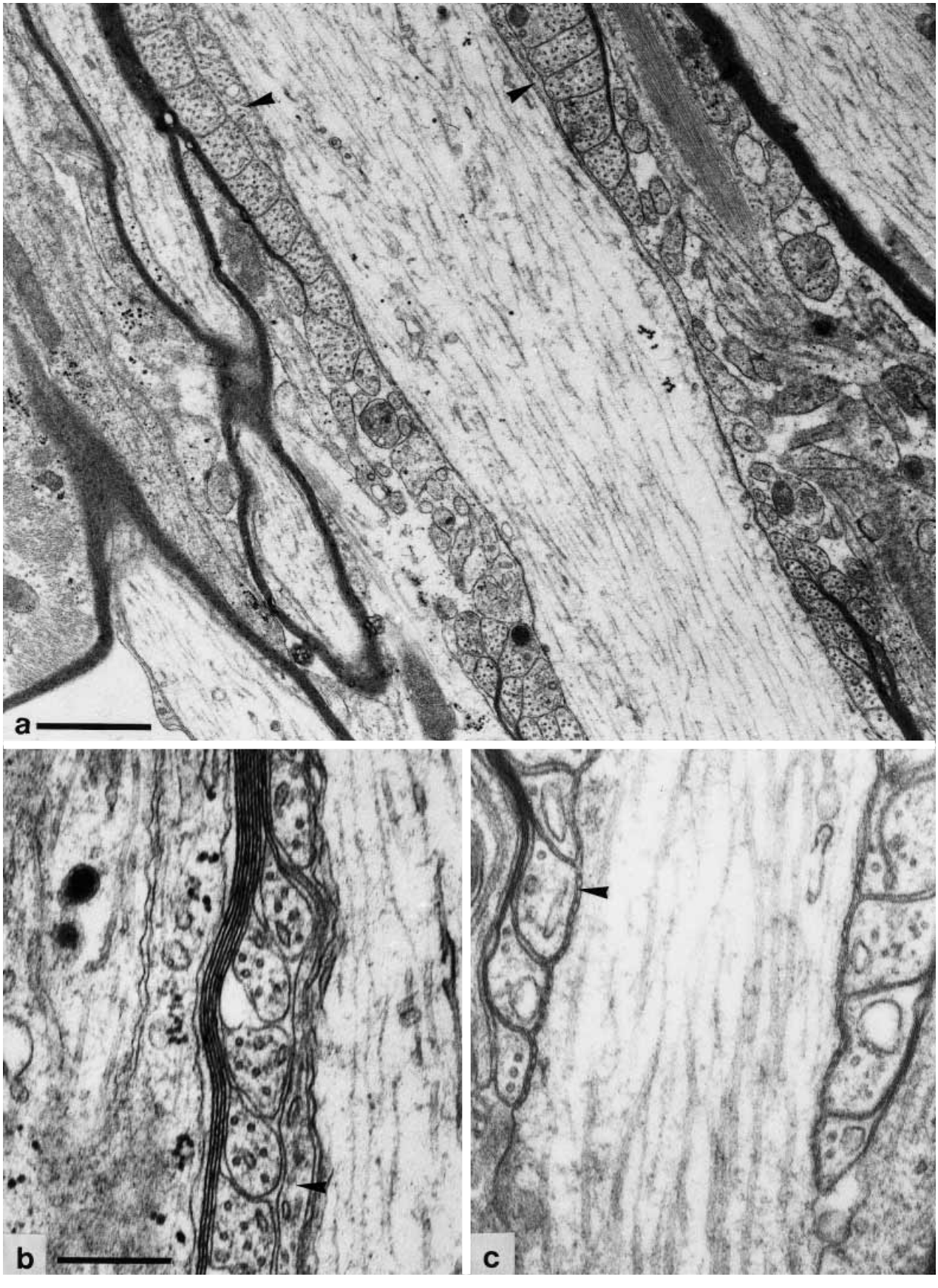

Fig. 5a–c

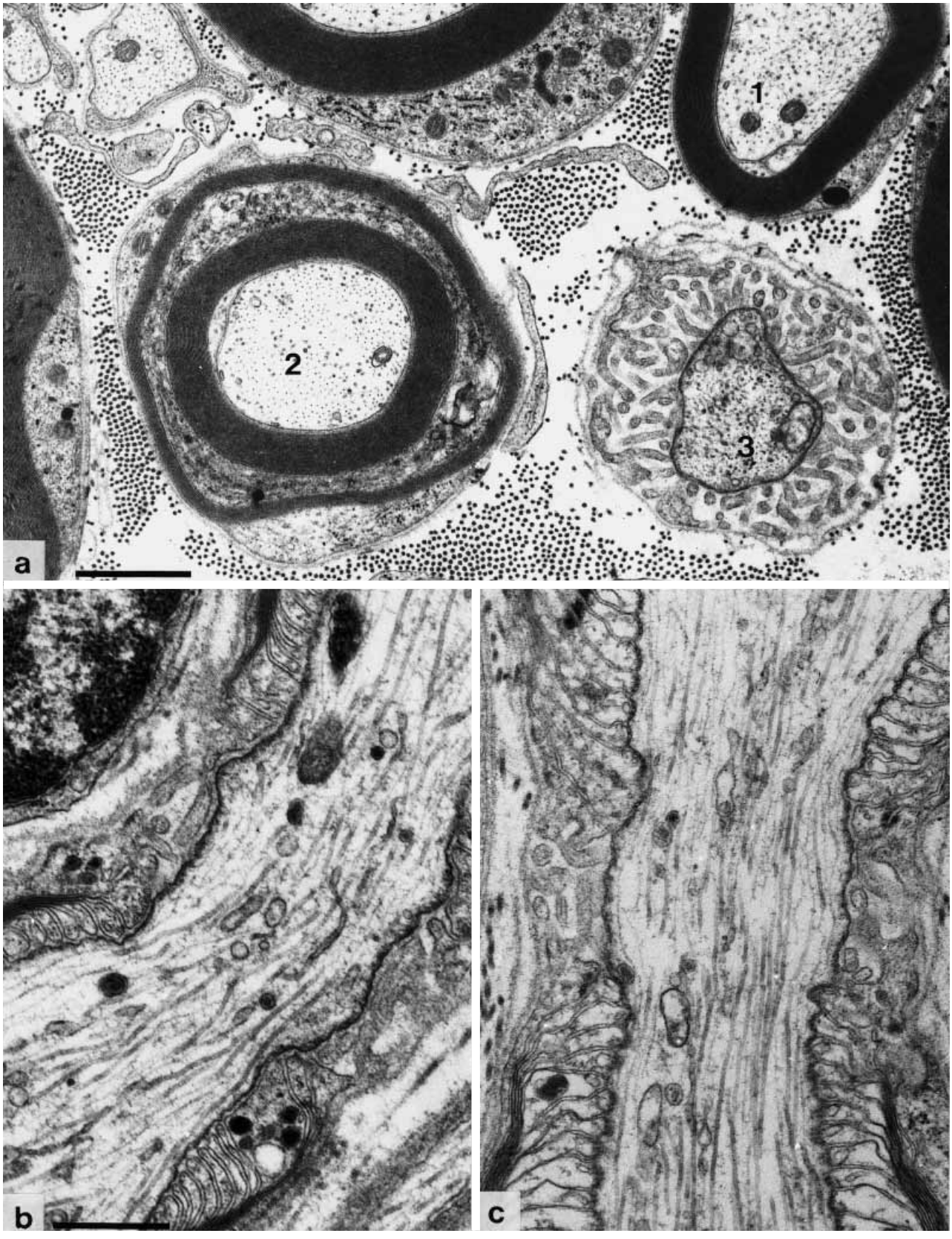

Fig. 6 **a** Cross section of sciatic nerve of a *cgt*$^{-/-}$ mouse. Normal, compacted myelin in the internode (*1*), in the region of a Schmitt-Lanterman incisure (*2*), and nodal region (*3*). Longitudinal sections of Ranvier nodes and paranodes of sciatic nerve show no morphological differences between the *cgt*$^{-/-}$ mutant (**b**) and the wild type (**c**). *Scale bars* **a** 1.2 μm, **b, c** 0.7 μm

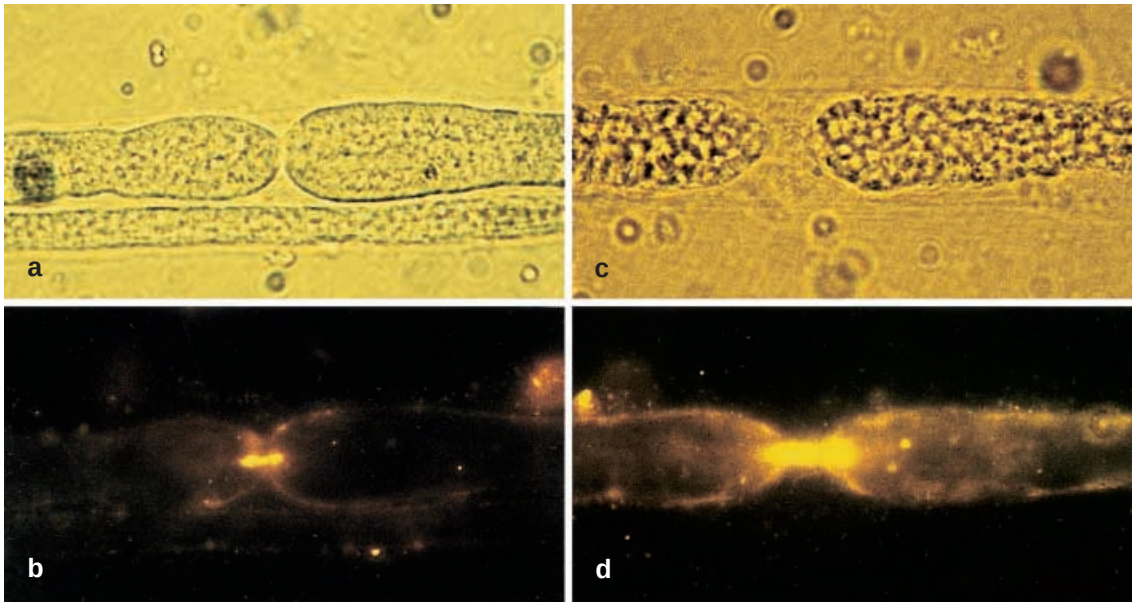

Fig. 7 Distribution of voltage-gated sodium channels in the axolemma of myelinated sciatic nerves of wild type (**a, b**) and *cgt*$^{-/-}$ (**c, d**) mice. **a, c** Phase-contrast images; **b, d** corresponding immunofluorescence images

slow, but not completely blocked conduction in the PNS of *cgt*$^{-/-}$ mice seems to be promoted by the low internodal sodium-channel concentration. A sodium-channel concentration as low as 2/μm^2 is sufficient for the conduction of an action potential in neonatal rat optic nerve (Waxman et al. 1989).

The results presented in this report have several implications: (1) cerebroside deficiency in the CNS leads to a hypomyelination similar but less severe to the phenotype of a dysmyelinosis originating in PLP mutations, e.g., jimpy mouse, md-rat, or Pelizaeus-Merzbacher. (2) We suggest that cerebrosides and sulfatides most likely play an important role in the correct targeting of axons by oligodendrocyte processes in the CNS. (3) Correctly folded and compacted myelin is formed without tight axonal contact in the CNS. (4) The loss of insulating properties due to severely altered physical properties of the lipid bilayer of GalC/sGalC-deficient myelin membranes leads to a dramatic loss of saltatory conduction.

References

Bansal R, Pfeiffer SE (1989) Reversible inhibition of oligodendrocyte progenitor differentiation by a monoclonal antibody against surface galactolipids. Proc Natl Acad Sci USA 86: 6181–6785

Bansal R, Gard AL, Pfeiffer SE (1988) Stimulation of oligodendrocyte differentiation in culture by growth in the presence of a monoclonal antibody to sulfated glycolipid. J Neurosci Res 21:260–267

Black JA, Kocsis JD, Waxman SG (1990) Ion channel organization of the myelinated fiber. Trends Neurosci 13:48–54

Boison D, Stoffel W (1994) Disruption of the compacted myelin sheath of axons of the central nervous system in proteolipid protein-deficient mice. Proc Natl Acad Sci USA 91:11709–11713

Bosio A, Binczek E, Stoffel W (1996a) Molecular cloning and characterization of the mouse CGT gene encoding UDP-galactose ceramide-galactosyltransferase (cerebroside synthetase). Genomics 35:223–226

Bosio A, Binzcek E, Le Beau MM, Fernald AA, Stoffel W (1996b) The human gene *cgt* encoding the UDP-galactose ceramide galactosyl transferase (cerebroside synthase): cloning, characterisation and assignment to human chromosome 4, band q26. Genomics 34:69–75

Bosio A, Binczek E, Stoffel W (1996c) Functional breakdown of the lipid bilayer of the myelin membrane in central and peripheral nervous system by disrupted galactocerebroside synthesis. Proc Natl Acad Sci USA 93:13280–13285

Bosio A, Binczek E, Stoffel W (1998) Composition and biophysical properties of myelin lipid define the neurological defects in galactocerebroside- and sulfatide-deficient mice. J Neurochem (in press)

Büssow H (1978) Schwann cell myelin ensheathing C.N.S. axons in the nerve fibre layer of the cat retina. J Neurocytol 7:207–214

Carenini S, Montag D, Cremer H, Schachner M, Martini R (1997) Absence of the myelin-associated glycoprotein (MAG) and the neural cell adhesion molecule (N-CAM) interferes with the maintenance, but not with the formation of peripheral myelin. Cell Tissue Res 287:3–9

Coetzee T, Fujita N, Dupree J, Shi R, Blight A, Suzuki K, Suzuki K, Popko B (1996a) Myelination in the absence of galactocerebroside and sulfatide: normal structure with abnormal function and regional instability. Cell 86:209–219

Coetzee T, Li X, Fujita N, Marcus J, Suzuki K, Francke U, Popko B (1996b) Molecular cloning, chromosomal mapping, and characterization of the mouse UDP-galactose:ceramide galactosyltransferase. Genomics 35:215–222

Curatolo W (1987) The physical properties of glycolipids. Biochim Biophys Acta 906:111–136

Diaz M, Bornstein MB, Raine CS (1978) Disorganization of myelinogenesis in tissue culture by anti-CNS antiserum. Brain Res 154:231–239

Dorfman SH, Fry JM, Silberberg DH (1979) Antiserum induced myelination inhibition in vitro without complement. Brain Res 177:105–114

Dugandzija-Novakovic S, Koszowski AG, Levinson SR, Shrager P (1995) Clustering of Na^+ channels and node of Ranvier formation in remyelinating axons. J Neurosci 15:492–503

Giese KP, Martini R, Lemke G, Soriano P, Schachner M (1992) Mouse P0 gene disruption leads to hypomyelination, abnormal expression of recognition molecules, and degeneration of myelin and axons. Cell 71:565–576

Hirano A, Dembitzer M (1967) A structural analysis of the myelin sheath in the central nervous system. J Cell Biol 34:555–567

Joe EH, Angelides K (1992) Clustering of voltage-dependent sodium channels on axons depends on Schwann cell contact. Nature 356:333–335

Kaplan MR, Meyer-Franke A, Lambert S, Bennett V, Duncan ID, Levinson SR, Barres BA (1997) Induction of sodium channel clustering by oligodendrocytes. Nature 386:724–728

Klugmann M, Schwab MH, Puhlhofer A, Schneider A, Zimmermann F, Griffiths IR, Nave KA (1997) Assembly of CNS myelin in the absence of proteolipid protein. Neuron 18:59–70

Li C, Tropak MB, Gerlai R, Clapoff S, Abramow-Newerly W, Trapp B, Peterson A, Roder J (1994) Myelination in the absence of myelin-associated glycoprotein. Nature 369:747–750

Molineaux SM, Engh H, Ferra F de, Hudson L, Lazzarini RA (1986) Recombination within the myelin basic protein gene created the dysmyelinating shiverer mouse mutation. Proc Natl Acad Sci USA 83:7542–7546

Montag D, Giese KP, Bartsch U, Martini R, Lang Y, Blüthmann H, Karthigasan J, Kirschner DA, Wintergerst ES, Nave KA, Zielasek J, Toyka KV, Lipp HP, Schachner M (1994) Mice deficient for the myelin-associated glycoprotein show subtle abnormalities in myelin. Neuron 13:229–246

Novakovic SD, Deerinck TJ, Levinson SR, Shrager P, Ellisman MH (1996) Clusters of axonal Na(+) channels adjacent to remyelinating Schwann cells. J Neurocytol 25:403–412

O'Brien JS, Rouser G (1964) The fatty acid composition of brain sphingolipids: sphingomyelin, ceramide, cerebroside, and cerebroside sulfate. J Lipid Res 5:339–342

Owens GC, Bunge RP (1990) Schwann cells depleted of galactocerebroside express myelin-associated glycoprotein and initiate but do not continue the process of myelination. Glia 3:118–124

Pascher I, Lundmark M, Nyholm PG, Sundell S (1992) Crystal structures of membrane lipids. Biochim Biophys Acta 1113: 339–373

Raine CS, Diaz M, Pakingan M, Bornstein MB (1978) Antiserum-induced dissociation of myelinogenesis in vitro. An ultrastructural study. Lab Invest 38:397–403

Ranscht B, Clapshaw PA, Price J, Noble M, Seifert W (1982) Development of oligodendrocytes and Schwann cells studied with a monoclonal antibody against galactocerebroside. Proc Natl Acad Sci USA 79:2709–2713

Ranscht B, Wood PM, Bunge RP (1987) Inhibition of in vitro peripheral myelin formation by monoclonal anti-galactocerebroside. J Neurosci 7:2936–2947

Roach A, Takahashi N, Pravtcheva D, Ruddle F, Hood L (1985) Chromosomal mapping of mouse myelin basic protein gene and structure and transcription of the partially deleted gene in shiverer mutant mice. Cell 42:149–155

Roberts DD (1986) Sulfatide-binding proteins. Chem Phys Lipids 42:173–183

Salzer JL (1997) Clustering sodium channels at the node of Ranvier: close encounters of the axon-glia kind. Neuron 18:843–846

Schulte S, Stoffel W (1993) Ceramide UDPgalactosyltransferase from myelinating rat brain: purification, cloning, and expression. Proc Natl Acad Sci USA 90:10265–10269

Schulte S, Stoffel W (1995) UDP galactose:ceramide galactosyltransferase and glutamate/aspartate transporter. Copurification, separation and characterization of the two glycoproteins. Eur J Biochem 233:947–953

Simons K, Ikonen E (1997) Functional rafts in cell membranes. Nature 387:569–572

Stoffel W, Boison D, Büssow H (1997) Functional analysis in vivo of the double mutant mouse deficient in both proteolipid protein (PLP) and myelin basic protein (MBP) in the central nervous system. Cell Tissue Res 289:195–206

Vabnick I, Novakovic SD, Levinson SR, Schachner M, Shrager P (1996) The clustering of axonal sodium channels during development of the peripheral nervous system. J Neurosci 16:4914–4922

Waxman SG, Ritchie JM (1993) Molecular dissection of the myelinated axon. Ann Neurol 33:121–136

Waxman SG, Black JA, Kocsis JD, Ritchie JM (1989) Low density of sodium channels supports action potential conduction in axons of neonatal rat optic nerve. Proc Natl Acad Sci USA 86:1406–1410